Depth sensing using coherence mapping

Estela Valero [a], Vicente Micó [b],*, Zeev Zalevsky [c], Javier García [b]

[a] *AIDO - Technological Institute of Optics, Color and Imaging, C/ Nicolás Copérnico 7-13, 46980, Paterna, Spain*
[b] *Departamento de Óptica, Universitat de Valencia, C/Dr. Moliner, 50, 46100 Burjassot, Spain*
[c] *School of Engineering, Bar-Ilan University, Ramat-Gan, 52900, Israel*

ABSTRACT

A method for depth sensing based on sensing the visibility associated with the coherence function of a laser source is presented. The setup is based on an electronic speckle pattern interferometric (ESPI) setup, where the object depth is encoded into the amplitude of the interference pattern without the need for depth scanning. After performing phase-shifting method, the object three-dimensional (3-D) shape is reconstructed by means as a range image from the visibility of the image set of interferograms and where each gray level represents a given object depth. Experimental results validate the proposed approach for reflective diffuse objects at different measurement distances.

© 2010 Elsevier B.V. All rights reserved.

1. Introduction

Nowadays, there are numerous applications that demand 3-D measurement of objects [1]. Just as an example, we find image encryption [2,3], object recognition [4,5] and 3-D mapping [6–8]. All of those possibilities have been allowed by the development of digital sensors and, in particular, by digital holography [9]. Digital holography offers highly attractive advantages such as high resolution, non-contact measurement, and versatility of implementation depending on the type of object. This way, digital holography has been applied to surface contouring of macro and small and micro-objects [10,11].

Other methods allow 3-D object shape by triangulation and can be presented under white light structured illumination [6] or under coherent illumination [12]. The general concept of triangulation is that the light projection and the observation directions are different. As the projected pattern is distorted by the object shape, the lateral positions of the measured pattern details include depth information of the object. But triangulation suffers from several problems: shadows incoming from the projection angle between illumination and detection directions, discontinuities and occlusions due to specific geometry of the object which generates additional shadowing and, thus, information losses. Moreover, the axial resolution of the system is limited by triangulation accuracy, and the method needs a wide measuring head for accurate measurements at long distances. One way to minimize the shadowing problems is to n-plicate the measurement system [13] or rotate the object [14]. The former

method implies both a high computational cost and expensive solution while the latter means a time consuming process to obtain the final result.

Another possibility to remove the shadow problem (not the occlusions) is to project the illumination on the same line that the observation direction. In this case, the spatially structured illumination will not help and an alternative coding must be used, most common being the time coding either in light pulse shape or in illumination spectral content. Examples are the time gating methods [15], time of flight [16], or the use of two wavelength illuminations [17]. Some of these techniques do not provide directly a 3-D mapping, but a contouring of the object. Although coaxial illumination and observation is complex to implement when considering conventional white light structured illumination, it is easy to achieve with coherent illumination because there is no need to project a structured illumination pattern onto the object surface: one can split the coherent beam before the object, illuminate the object coaxially with the observation direction and reinsert a reference beam at the digital recording device. This is the underlying principle of electronic speckle pattern interferometry [18]. Basically, phase-shifting and Fourier transformation are the two main methods to recover the object phase distribution and correspond with on-axis and off-axis reference beam reinsertion geometry, respectively [19,20]. However, both procedures allow access to the wrapped phase distribution of the object (as is the case in contouring methods) that is, phase values lying in the range of −π to π, as a consequence of the depth-to-phase coding. The phase map needs to be unwrapped to recover the 3-D object information. Once again, phase-unwrapping algorithms will not be useful if the image contains unknown relative heights and/or the object contains sudden jumps on its profile, that is, discontinuities, occlusions and/or shadows.

---

* Corresponding author. Tel.: +34 963 544 097; fax: +34 963 544 715.
 E-mail address: vicente.mico@uv.es (V. Micó).

Different approaches had been proposed to avoid the phase-ambiguity problem. Thus, Saldner and Huntley proposed a method named as temporal phase unwrapping where the basic idea is to vary the pitch of the projected fringes over time [21]. They evaluated independently the object phase at each pixel in order to provide an absolute measurement of the surface height. Thus, by recording a sequence of phase maps, a 3-D phase distribution is obtained by unwrapping the phase at each pixel along the time axis. This procedure yields on an absolute measurement of the object surface height. On the other hand, Sjödahl and Synnergren solved the discontinuity problem of the phase map by means of the projection of a random pattern instead of periodic fringes [22]. Since the intensity of a random pattern varies without a regular period, every small region in the projected pattern becomes unique. Using an initial calibration process of the projected random pattern along the working volume, it is possible to trace the movement of each small region at the detector by simple correlation algorithm when the object under study is illuminated by such random pattern. Thus, assuming that the motion of every small area can be detected, the 3-D object shape can be retrieved. However, Sjödahl and Synnergren used a white light optical projector and an optical triangulation architecture, that is, the measured object shape suffers from previously commented problems.

Another way to project a random pattern is by using the speckle patterns that happen when coherent light is reflected or transmitted from a rough surface. García et al reported a novel approach to 3-D measurement by projecting the random speckle pattern through a ground glass diffuser [23]. In this approach, inherent changes in propagation of the speckle pattern will uniquely characterize each specific location in the working volume in such a way that it is possible to determine the 3-D object map by analyzing the speckle pattern itself (not that one produced by the object). This procedure allows the representation of the 3-D object shape in a range image composed by gray levels in which each level is representative of an object depth. Aside the novelty of the method, it defines a resolution which is independent of the object observation distance or the angle between the illumination and the observation direction because it is based on local correlations of speckle patterns. Moreover, no shadowing problem is produced because it can be performed using parallel architecture between illumination and detection. Also, the proposed method was validated for transparent samples and reflective diffuse objects.

Other interesting methods solve the discontinuity problem of the phase map are based in the coherence of the light source. Coherence coding has been applied to spatial information transmission and superresolution [24–26], optical coherence tomography [27,28], and 3-D topography in digital holographic microscopy [29,30]. Last year, Yuan et al introduced a new approach to achieve 3-D surface contouring of reflecting micro-objects [31]. They proposed a digital lensless Fourier holographic system with a short coherence light source that can be used to record different layers of a micro-object through changing the object position. Thus, by bringing into the coherence spatial interval different sections of the object, it is possible to digitally reconstruct the whole 3-D surface contouring of the object. This approach takes the advantage provided by a limited source coherence length which allows optical sectioning of the 3-D object profile.

And recently, Zalevsky et al. presented a new method for 3-D imaging based on partial coherence in digital holography [32]. In their paper, Zalevsky et al. reported on two different approaches both of them aimed to remove the phase ambiguity problem in digital holography. In one of the proposed concepts, they achieve 3-D profile of a reflective object using an approach based on illuminating the object with a light source having a relatively long coherence length. As the contrast of the fringes within this length will vary, this fact can be used for 3-D estimation after performing a calibration of the contrast of the interference fringes in the whole coherence length axial interval. Thus, by comparing the contrast of the fringes provided by the object with that

one obtained in the calibration process, they were able to extract 3-D information. They proposed a lensless digital holographic optical setup in which no lenses are needed to image the input object because the approach is focuses on mapping the 3-D information of reflective objects. This fact disables the reported approach when diffuse objects are considered. Moreover, because of the lensless geometry, there will be restrictions between the observation distance and the object size in order to optimize the space-bandwidth product of the system.

In this paper, we present a novel approach in which we take profit on the change in visibility of the interference speckle pattern in 3-D space incoming from a relatively long but limited source coherence length. When a classical ESPI configuration is considered, the object areas falling inside the coherence volume range of the illumination source will produce speckle interference with the reference beam. A phase modulation of the reference will result in blinking intensity only for those points inside the coherence range. Thus, the proposed approach performs coherence-to-depth coding of the 3-D object shape in such a way that the 3-D object information is related with the amplitude of the speckle interference. And the way to decode such information coding is by computing the visibility of the speckle interference along the whole volume range. After some digital post-processing to smooth speckle noise, it is possible to get a range image where each gray level contains information of a different object depth. The proposed approach has three major advantages. First, the resolution of the method does not depends on the observation distance because the coherence volume range can be easily tuned from near to far distance by simple adding optical path in the reference beam. Second, no shadowing problem is produced because the illumination and observation directions are collinear. And third, as the method implies the obtaining of a range image, there is no problem with sudden jumps or occlusions in the object shape. In addition, unlike other coherence based methods like optical coherence tomography, the proposed method does not require axial distance or wavelength scanning.

The paper is organized as follows. Section 2 presents the methodology and explains the underlying principle of the proposed approach. In Section 3 we present an experimental validation of the method for short and large measurement distances and Section 4 concludes the paper.

2. Description of the optical setup and operating principle

To test the capabilities of the proposed method from an experimental point of view the basic setup depicted in Fig. 1 has been assembled in the laboratory. It is a classical ESPI configuration. Light coming from a laser source is split into reference and illumination beams. The illumination beam reaches the 3-D object after being spatially filtered and projected onto it. Notice that, in this configuration, the illumination direction is not strictly collinear with the observation one. This fact does not imply a restriction because it is possible to illuminate using the beam splitter just before the imaging system. However, to gain in simplicity and to better matching the optical paths, we have selected the depicted configuration.

Thus, a diffuse reflective object is illuminated by a light beam having a given coherence length. And at the same time, a reference beam is inserted in on-axis mode onto the detection plane with a divergence that equals that one provided by the 3-D object. So, an on-axis hologram having no carrier frequency fringes but dominated by speckle is recorded by the CCD. Taking into account that the coherence length of the illumination light is relatively long, it is possible to well-match the optical path length of the reference beam in such a way that the whole object depth falls inside half the coherence length interval. In this case, different speckles coming from different depths of the 3-D object will interfere with different amplitude once they are imaged by the CCD camera. We can say the proposed approach is performing a coding of the 3-D object depth into the coherence of the illumination
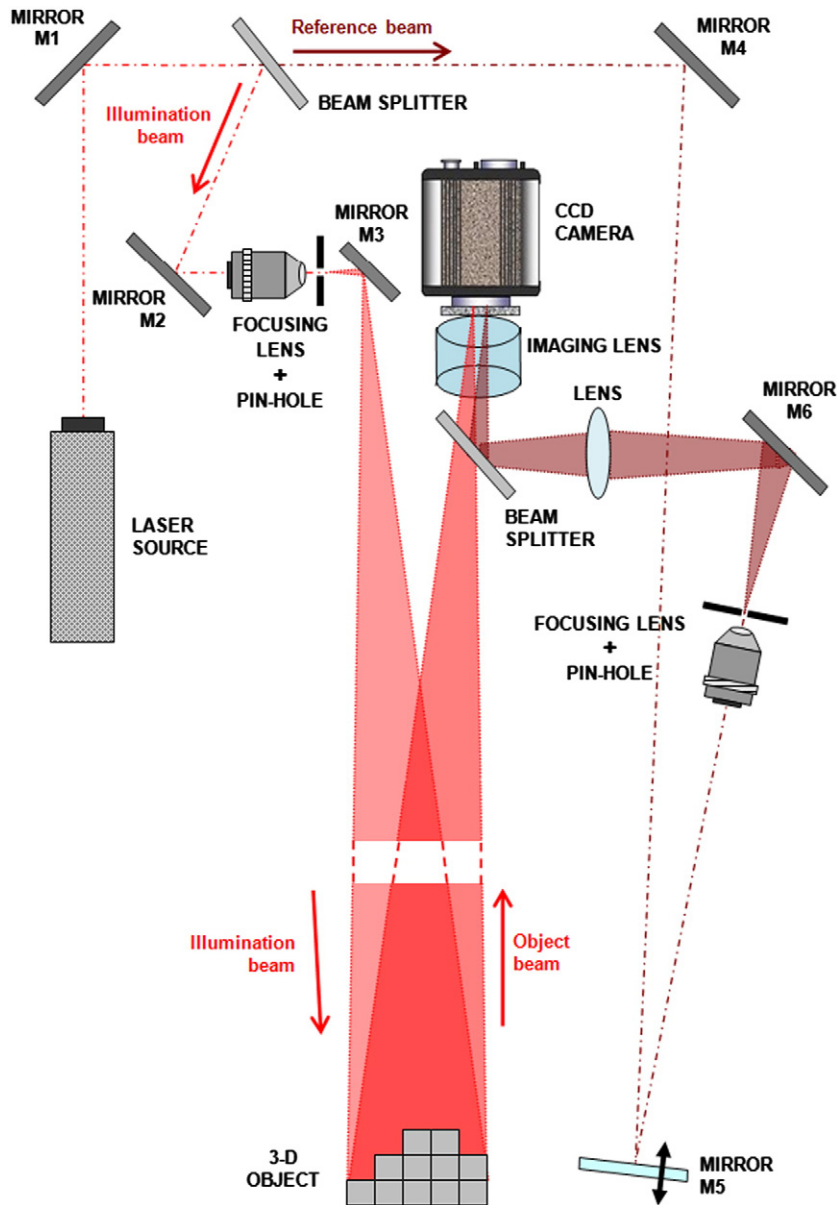
Fig. 1. T-ESPI experimental setup used for validation of the proposed approach. The discontinuity in both illumination and object beams is representative of the arbitrary distance between 3-D object and imaging device. The mirror M5 is a piezo-electrical one to provide phase-shifting procedure.

light since the 3-D object information is related with the amplitude of the speckle interference.

In order to evaluate such variable amplitude with the distance when considering different regions of the 3-D interference object field of view, we introduce a slow perturbation in time at the reference beam, that is, a temporal phase-shifting, by using a piezo-electric mirror. Thus, computing the visibility of the recorded set of interferograms it is possible to finally obtain a range image where each small area of the 3-D object is represented by a given gray level incoming from the coherence-to-depth encoding that has been performed. And this range image becomes a 3-D mapping of the object under test.

Additionally, by mapping the whole coherence volume with a reference object (a plane calibration plate, for instance) in order to obtain the visibility of the interference versus axial position, we can obtain a gray level chart corresponding with different depths in the working volume. This record will make the depth calibration of the system. Thus, once the range image is obtained, it is possible to directly assign each gray level to a given depth, and the 3-D information of the object under test becomes recovered.

Considering now the proposed approach from a theoretical point of view, we can say that the resulting field distribution impinging at the CCD when considering two interference beams in on-axis mode is

$$A(x,y;t) = A_1 \exp(i\phi_1(t)) + A_2 \exp(i\phi_2(t)) \tag{1}$$

where A_i, ϕ_i are the amplitude and phase distributions of each beam, respectively. Then, the CCD performs intensity recording, that is

$$I(x,y;t) = |A(x,y;t)|^2 = A_1^2 + A_2^2 + 2A_1A_2\langle \cos(\phi_1(t)-\phi_2(t))\rangle \tag{2}$$

where $<....>$ designates time averaging operation in a time span comparable to the inverse of the optical frequencies. Just as examples, if both beams are fully coherent: $\langle\cos(\phi_1(t)-\phi_2(t))\rangle = \cos(\phi_1(t)-\phi_2(t))$, while if both beams are incoherent: $\langle\cos(\phi_1(t)=\phi_2(t))\rangle = 0$. Therefore it is clear that the degree of coherence determines the contrast of the interference. Defining γ as the degree of temporal coherence, it is clear that two completely coherent or incoherent beams can be represented by $\gamma=1$ and $\gamma=0$, respectively. In our case, the

degree of temporal coherence is a function of the axial distance since we are making interference between different reflected beams incoming from different axial positions. So, considering $\gamma = \gamma(z)$, Eq. (2) can be rewritten as

$$I(x,y,z;t) = I_1 + I_2 + 2\sqrt{I_1 I_2}\gamma(z)\cos[\phi(t)] = I_T\{1 + V_0(t)\gamma(z)\cos[\phi(t)]\}$$
(3)

where $\phi(t) = \phi_1(t) - \phi_2(t)$ is the phase difference between both interferometric beams at a given instant, $I_i = A_i^2$ the intensity of each beam and $I_T = I_1 + I_2$ is the total intensity in case of incoherent addition of the beams. Notice that $V_0 = 2\sqrt{I_1 I_2}/(I_1 + I_2)$ is the visibility of the recorded interference pattern in case of perfect coherence, while $V = V_0\gamma(z)$ gives the full visibility which comprises the effects of beam ratio and coherence.

Eq. (3) shows that the degree of temporal coherence modulates the total intensity recorded at the CCD detector in such a way that different object depths will produce a different intensity in the recorded interferogram as we are mapping the coherence volume of the illumination light. Thus, it is possible to obtain a range image of the 3-D object by determining the interference visibility and from this value the degree of temporal coherence $\gamma(z)$.

To do this, we capture the object and reference beam separately by alternately occluding each of the beams. This gives two reference images (I_1 and I_2) with the spatial distribution of reference and object beams. Then for obtaining the visibility (V) of the interference pattern, we capture a sequence of phase-shifted interferograms. This is performed by recording a video sequence and applying a time varying phase to the reference arm. With the values of I_1, I_2 and V the value of $\gamma(z)$ is computed for each pixel as $\gamma(z) = V/V_0$. With this procedure, we obtain an image which is proportional to the degree of temporal coherence, which is related to the object depth. This process in performed for a calibration plate giving a relation between gray level and depth. Finally, the profile of the object can be estimated by comparing the result of degree of coherence with the gray level chart obtained by calibration.

The visibility extraction can be performed without any particular phase shifting pattern on the reference arm. Note that, eventually, only the minimum and maximum intensities for each point are needed, regardless the phase which achieve those values. Even if a random phase is applied over the reference, it is enough to grab enough number of interferograms so that maximum and minimum possible intensities are obtained for each camera pixel. Obviously this is hard to warrant in case of random phase shift, but simple for a linear phase, which is easily achieved by means of a piezo-mirror connected to a function generator, as shown in Fig. 1. The recording interval is larger than the period of the modulation function in the piezo-mirror. In case of a linear phase the intensity for each pixel can be fit to a sinusoidal function [Eq. (3)] giving as a result higher accuracy in the visibility calculation and so to reduce the noise.

It is important to stress that, despite the need for several frames (at least 3) the method does not relies on scanning over the depth or the wavelength. The multiple frames are used just for determining the contrast of the interferences. Thus, the expected range for depth is given by the coherence length of the light used, while the accuracy will be governed by the stability in the coherence shape of the light source and the noise introduced by the system. In contrast, in an OCT based system the accuracy is determined by the coherence length and the range by the scanning range, either in wavelength or in axial distance. In our case, a major noise source is the speckle [33], because the system is based on a coherent imaging system.

3. Experiments

3.1. Validation and calibration

Fig. 2 images a picture of the experimental setup assembled at the laboratory for the short measurement distance case and for calibration. Objects are placed at a distance of 90 cm approximately in front of an imaging system composed by an imaging lens (50 mm focal length video lens) and a CCD camera (Kappa DC2, 12bits dynamic range, 1352 × 1014 pixels with 6.7 μm pixel size). A He–Ne laser source (632.8 nm wavelength) is used as illumination light in the experimental setup. The coherence function is dominated by the inhomogeneous Doppler broadening that gives a Gaussian coherence profile with a width of 20 cm approximately according to the laser manual.

In a first step we will perform a testing of the method by using a planar calibration plate. For the calibration we use the same experimental setup depicted in Fig. 2 but using a diffusive plate as test object. The plate normal is aligned with the line of sight and is translated along the said line of sight during calibration. The set of axial location of the plate includes the location at null optical path difference between reference and imaging arms (which will provide maximum visibility interference). This location distance is considered as origin for axial
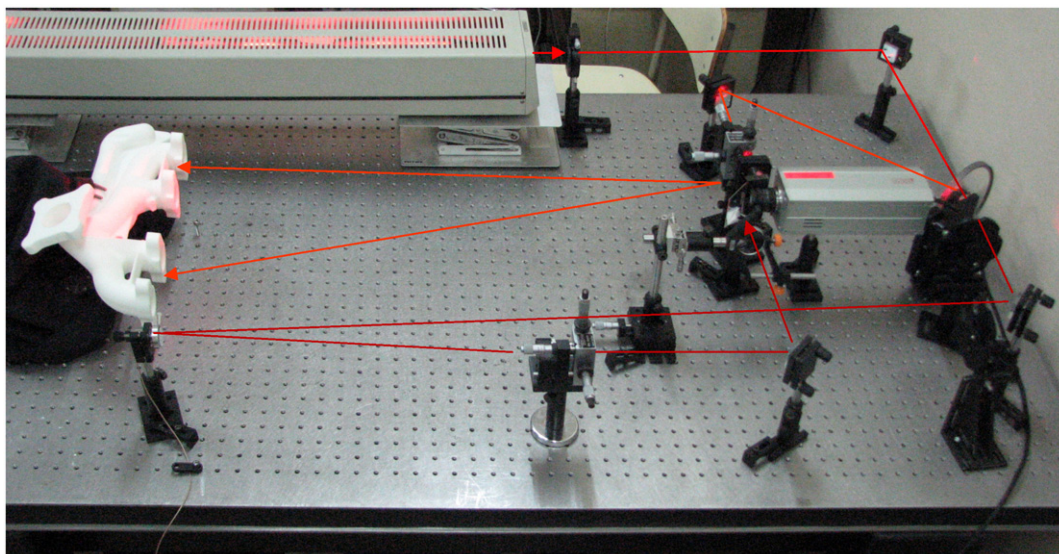

Fig. 2. The experimental setup assembled at the laboratory for measurements at short distance where the main optical paths of both beams are depicted for clarity. The different components depicted in Fig. 1 can be easily identified in the image where additional neutral filters are included for intensity beam ratio adjustment.
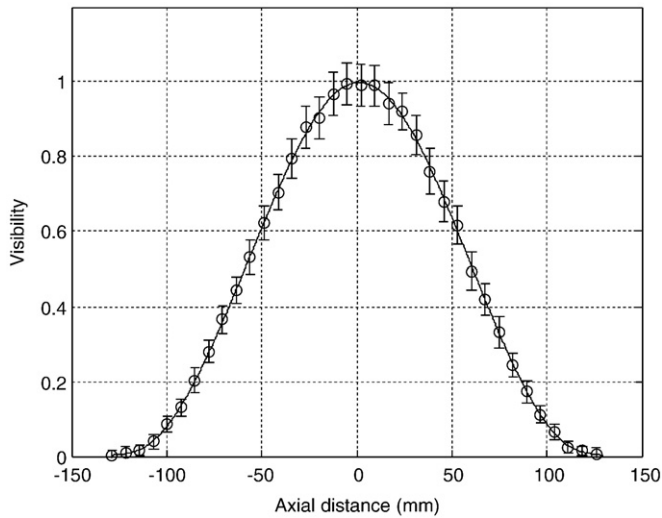
Fig. 3. Calibration curve: visibility averaged over a weighted window with diameter of 5 pixels for different axial distances.

distances. As the calibration plate is progressively farer from the origin the visibility is expected to diminish following the coherence function of the light source. As explained in the previous section, a set of images with variations in the reference phase by means of a piezo-mirror are taken and the visibility is extracted in each image point. This calibration process could be performed for any measurement distance in order to properly match the visibility of the reflected speckle pattern with the center of the Gaussian coherence profile.

Fig. 3 shows the visibility extracted as a function of the depth around the equal path length point. Owing to the inherent coherent noise from the speckle imaging, the visibility for a single point would suffer excessive noise. Instead a spatial averaging (smoothing) over a small size window is needed. We use a smoothing with a Gaussian window with size (half width at medium height) of 5 pixels. This still renders high lateral resolution and reasonable axial resolution. As can be seen from the calibration curve, an axial range of approximately 120 mm can be mapped at each side of the origin without ambiguity. For each axial location in the calibration the standard deviation is also plotted. Note that increasing the averaging window size would give an enhanced axial resolution, but at the expense of a diminished lateral resolution. The accuracy can be roughly estimated from the calibration curve as 10 mm approximately. Note that the accuracy will be higher for a larger averaging window. There is a tradeoff between spatial resolution and axial accuracy. An increase of spatial resolution in the detector (number of pixels) can be used to reduce the speckle size, which permits to increase lateral resolution without compromising accuracy. So, the image resolution results the basic limiting factor for the precision of the method.

3.2. Short range measurement

The same setup as for calibration is used for short range mapping. Fig. 4 images the two objects used to test the proposed method in both cases, short and long measurement distance. One is a 3-D sample built from singles blocks of a toy object and the other one is a gas collector prototype of an engine. The blocks in the first case permit the construction of an object with steps separated by 16 mm in depth. Note in this object as the hole in the lower part, which is closed in the back side, gives a rectangular hole with also 16 mm depth with respect to the borders.

Fig. 5 shows the reconstruction obtained for the objects in Fig. 4. Fig. 6 depicts a 3-D plot of the relief for the Blocks object. It is especially noticeable the ability to map the inside of the holes facing the camera. This situation happens for both objects and demonstrates the absence of shadow problem with this method.
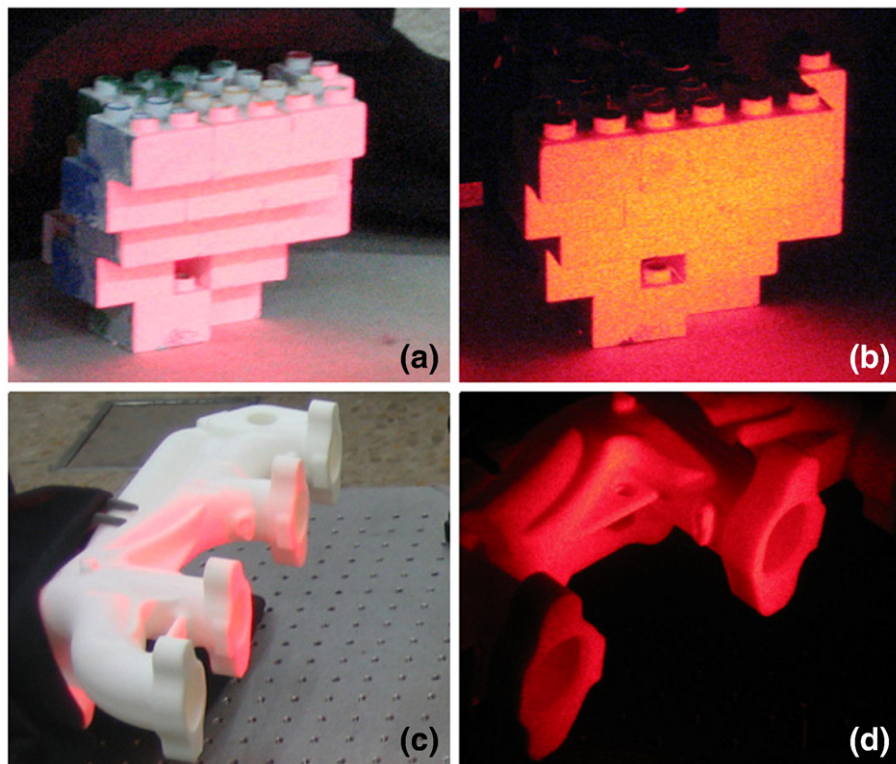

Fig. 4. Objects used in the experimental validation of the proposed approach: (a)–(b) and (c)–(d) are a 3-D object composed by building blocks (Blocks) and a gas collector prototype of an engine (Collector), respectively.
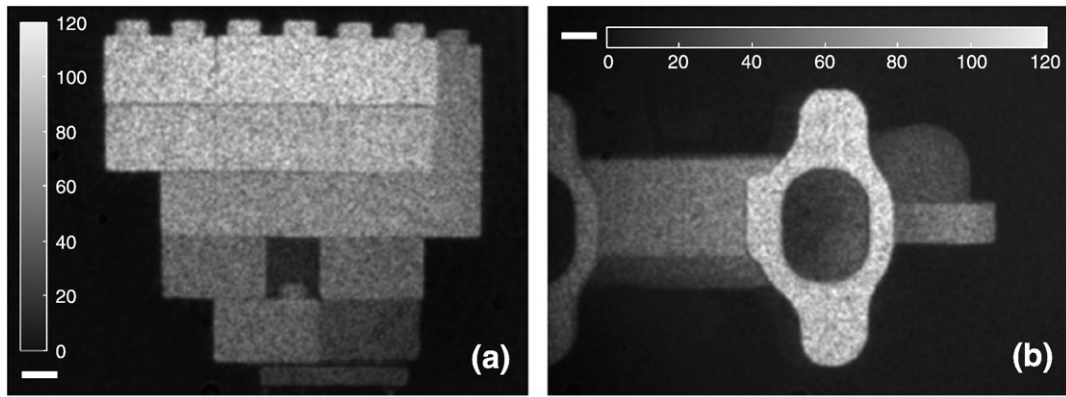
Fig. 5. Mapping obtained for the objects in Fig. 4 when positioned at short distance (0.9 m). (a) Blocks. (b) Collector. Scale-bar size is 10 mm. Units in mm.
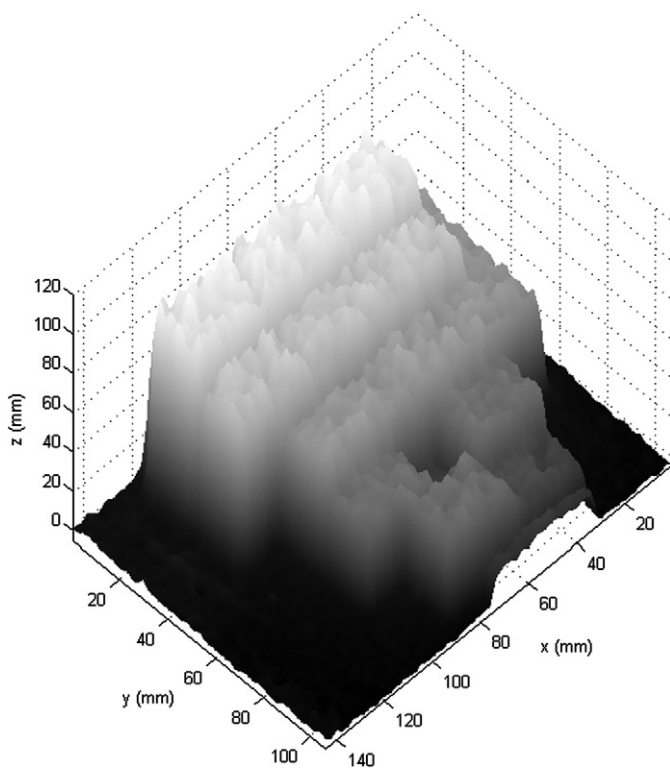

Fig. 6. 3-D plot of the mapping obtained for the Blocks object.

3.3. Long range measurement

For long range measurements the objects where located at 5 m approximately from the camera (limited by the laboratory size). The system is rearranged to add this distance to the reference arm by means of a delay line, providing a neat interference speckle pattern from the object. Additionally a longer focal length imaging lens is used, in order to provide a similar field of view as in the short range case. The resulting images are depicted in Fig. 7. As can be seen, aside of the scaling factor due to different imaging magnification, the results are analogous to those obtained at short distances. Again the lack of shadowing is patent as well. It is worth noticing that the additional distance between the system and the object does not introduce any change in the performance of the method.

4. Conclusions and discussion

We have presented a novel approach for 3-D diffuse object mapping based on the degree of temporal coherence of the interference speckle pattern reflected by the object. Because of each small area in the coherence volume of the illumination source will produce an interference pattern with different amplitude, it is possible to estimate the 3-D object shape by computing the visibility of recorded interference pattern. This process can be understood as a coherence-to-depth coding of the 3-D object shape in such a way that the 3-D object information is related with the visibility of the speckle interference. After performing the proposed approach, the 3-D object information is recovered in a range image where the different gray levels are representative of a different object depth. Experimental results validate the proposed concept considering two experimental
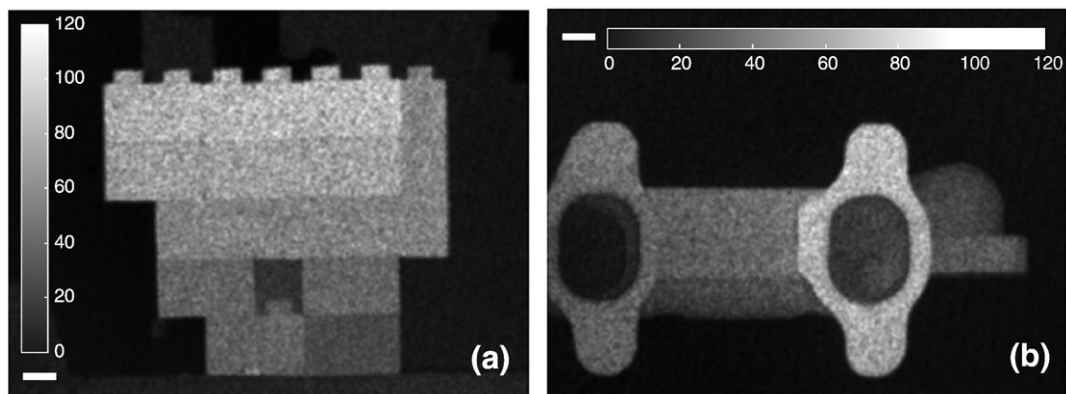

Fig. 7. Mapping obtained for the objects in Fig. 4 when positioned at long distance (5 m). (a) Blocks. (b) Collector. Scale-bar size is 10 mm. Units in mm.

configurations having different measurement distances. Since the depth value is obtained from normalized intensity values the measurement does not depend directly on the objects reflectivity of surface characteristics. Nonetheless, in the extreme cases, a low reflectivity or non diffuse object will produce low intensity values, resulting in less accurate measurements. In general, the measurement accuracy can be enhanced by applying a diffusive white paint on the object, as is common in many 3D capturing systems.

Another important capability of the proposed method is that its accuracy and range is dependent on the coherence length of the illumination laser light. Since the classical coherence shape of a laser is a Gaussian distribution, the narrower the Gaussian function, the better the axial resolution. As we find a lot of lasers with different coherent length ranges, the selection of the laser source could be application dependent. Thus, we can choose a short coherence length (in the range or microns) to achieve high accuracy in microscopic applications or we can select a longer coherence length (from several centimetres to upwards) for macroscopic object digitization, range estimation and so on. Although methods for temporal coherence shaping could be used permitting the use of a single laser, this would greatly complicate the setup. Therefore, in practice the laser selection limits the specific system to a given application and reduces the versatility of the technique.

The proposed method has unique advantages in comparison with other approaches for 3-D mapping: it has no dependence in resolution with the observation distance as in the case of triangulation methods, it has no problems with sudden jumps in the object shape as in the methods that implies wrapped phase distribution of the object, and it has no shadow illumination problem and minimization of the occlusion one because the illumination and imaging recording can be performed from the same location.

References

[1] F. Chen, G.M. Brown, M. Song, Opt. Eng. 39 (2000) 10.
[2] O. Matoba, B. Javidi, Opt. Lett. 24 (1999) 762.
[3] E. Tajahuerce, B. Javidi, Appl. Opt. 39 (2000) 6595.
[4] T. Poon, T. Kim, Appl. Opt. 38 (1999) 370.
[5] J.J. Esteve-Taboada, J. García, C. Ferreira, Appl. Opt. 39 (2000) 5998.
[6] M. Takeda, K. Mutoh, Appl. Opt. 22 (1983) 3977.
[7] V. Srinivasan, H.C. Liu, M. Halioua, Appl. Opt. 23 (1984) 3105.
[8] W.H. Su, Opt. Express 15 (2007) 13167.
[9] U. Schnars, W. Jüptner, Appl. Opt. 33 (1994) 179.
[10] G. Pedrini, P. Fröning, H.J. Tiziani, F.M. Santoyo, Opt. Commun. 164 (1999) 257.
[11] C. Quan, X.Y. He, C.F. Wang, C.J. Tay, H.M. Shang, Opt. Commun. 189 (2001) 21.
[12] G. Indebetouw, Appl. Opt. 17 (1978) 2930.
[13] W. Su, Ch. Kuo, Ch. Wang, Ch. Tu, Opt. Express 16 (2008) 4069.
[14] M. Halioua, R.S. Krishnamurthy, H. Liu, F. Chiang, Appl. Opt. 24 (1985) 2193.
[15] G.J. Iddan, G. Yahav, Proc. Soc. Photo-Optical Instrum. Eng. 4298 (2001) 48.
[16] N. Abramson, Appl. Opt. 30 (1991) 1242.
[17] B.P. Hildebrand, K.A. Haines, J. Opt. Soc. Am. 57 (1967) 155.
[18] R.S. Sirohi, Speckle metrology, Marcel Dekker, New York, 1993.
[19] I. Yamaguchi, T. Zhang, Opt. Lett. 22 (1997) 1268.
[20] J.M. Huntley, in: P.K. Rastogi (Ed.), Digital speckle pattern interferometry and related techniques, Wiley, 2001, p. 59, Ch. 2.
[21] H.O. Saldner, J.M. Huntley, Appl. Opt. 36 (1997) 2770.
[22] M. Sjödahl, P. Synnergren, Appl. Opt. 38 (1999) 1990.
[23] J. García, Z. Zalevsky, P. García-Martínez, C. Ferreira, M. Teicher, Y. Beiderman, Appl. Opt. 47 (2008) 3032.
[24] B.J. Guo, S.L. Zhuang, Appl. Opt. 30 (1991) 5159.
[25] Z. Zalevsky, J. García, P. García-Martínez, C. Ferreira, Opt. Lett. 30 (2005) 2837.
[26] V. Micó, J. García, C. Ferreira, D. Sylman, Z. Zalevsky, Opt. Lett. 32 (2007) 736.
[27] D. Huang, E.A. Swanson, C.P. Lin, J.S. Schuman, W.G. Stinson, W. Chang, M.R. Hee, T. Flotte, K. Gregory, C.A. Puliafito, J.G. Fujimoto, Science 254 (1991) 1178.
[28] A.F. Fercher, C.K. Hitzenberger, Prog. Opt. 44 (2002) 215.
[29] P. Massatsch, F. Charrière, E. Cuche, P. Marquet, C.D. Depeursinge, Appl. Opt. 44 (2005) 1806.
[30] L. Martínez-León, G. Pedrini, W. Osten, Appl. Opt. 44 (2005) 3977.
[31] C. Yuan, H. Zhai, X. Wang, L. Wu, Opt. Commun. 270 (2007) 176.
[32] Z. Zalevsky, O. Margalit, E. Vexberg, R. Pearl, J. García, Appl. Opt. 47 (2008) D154.
[33] J.W. Goodman, Speckle Phenomena in Optics, Roberts and Co., 2006.